Electronic Supplementary Material (ESI) for Lab on a Chip.

Supplementary Information

NAIL: **N**ucleic **A**cid detection using **I**sotachophoresis and **L**oop-mediated isothermal amplification

Mark D. Borysiak[a], Kevin W. Kimura[a], and Jonathan D. Posner*[ab]

[a] Department of Chemical Engineering, University of Washington, Seattle, WA 98195

[b] Department of Mechanical Engineering, University of Washington, Seattle, WA 98195

*Corresponding Author, Email: jposner@uw.edu

Abstract

The supporting information describes the capillary burst valve, separation capacity calculations, hydraulic resistance calculations, device fabrication details, LAMP primer sequences, example images of LAMP reactions, a limit of detection plot with 95% confidence intervals, and a summary of limit of detection results.

.

Capillary valve pressure

The capillary valve pressure given by the modified Young-Laplace equation from Cho et al,

$$P_A - P_0 = -2\sigma\left(\frac{\cos(\theta_A+\beta)}{b}+\frac{\cos\theta_A}{h}\right), \quad (1)$$

is dependent upon the valve width, b, diverging wall angle, β, height of the channel, h, surface tension of the liquid, σ, and the contact angle of the liquid on the substrate surface, θ_A.[1] The capillary valve uses a diverging wall characterized by an angle β to effectively increase the contact angle of the flowing solution and create an energetic barrier to further flow. The pressure drop created by the bulging liquid-gas interface at the diverging wall, P_A–P_0, must be exceeded by an external pressure to overcome the energetic barrier created by the bulging interface and allow the fluid to continue advancing along the diverging walls. The maximum contact angle that a liquid meniscus can attain is 180°, so for $\theta_A+\beta > 180°$, the valve will burst when the liquid advances to a contact angle of 180° on the original wall. Figure S1 shows a graphic of a capillary valve with a diverging angle of β =90°.

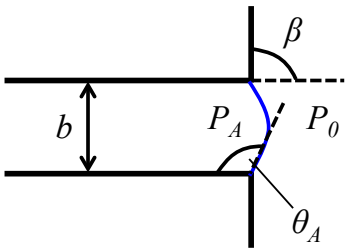

Figure S1. Schematic of the capillary burst valve with a bulging liquid interface at a diverging wall. The pressure inside the liquid, P_A, and outside the liquid P_0, are shown. The valve width, b, the advancing contact angle of the liquid on the substrate, θ_A, and the diverging wall angle, β, are also shown.

Tween-20 in the leading electrolyte (LE) affects both the surface tension and the contact angle of the liquid on the substrate. Niño and Patino give the surface tension of tween-20 in water at various concentrations,[2] while the contact angle of the LE solution on air plasma treated SEBS, θ_A, was measured using contact angle goniometry. Figure S2 shows the effect of tween-20 concentration on the valve pressure at constant valve width (75 μm), height (170 μm), and diverging angle (120°). The valve pressure decreases with increasing tween-20 concentration due to decreased surface tension and more hydrophilic contact angle. Figure S2 also shows the effect of valve width and diverging angle on the valve pressure at constant tween-20 concentration (0.001%) and height (170 μm). The valve pressure decreases with increasing width and decreasing diverging angle. We observed that a valve pressure of approximately 800 Pa was necessary to prevent bursting prior to the end of ITP experiments. We used a valve width of 75 μm, height of 170 μm, diverging angle of 120°, and tween-20 concentration of 0.001% to give a valve pressure of approximately 900 Pa.

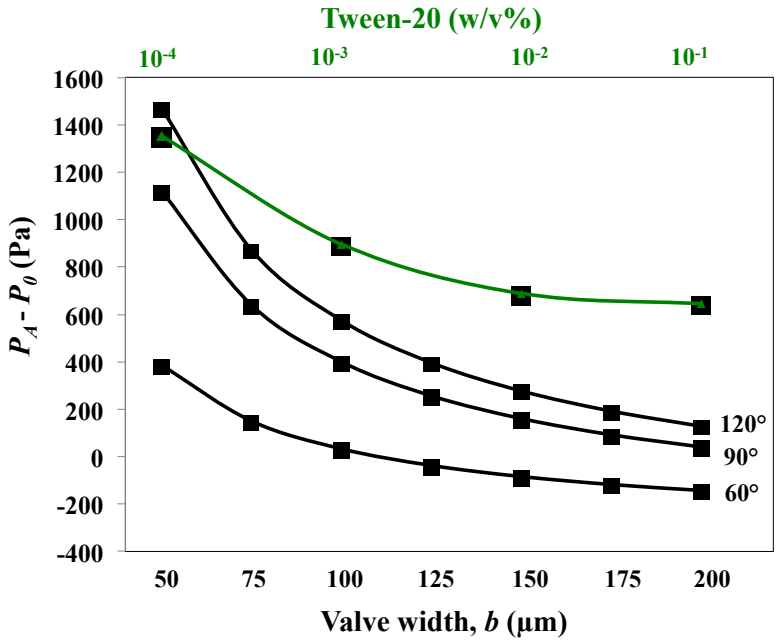

Figure S2. Effect of tween-20 concentration (w/v%), valve width, and diverging angle on valve pressure. The green line (triangles) shows the effect of tween-20 concentration (top abscissa) on the valve pressure at constant width (b=75 μm), height (h=170 μm), and diverging angle (β=120°). Increasing tween-20 concentration gives smaller valve pressures due to smaller contact angles on SEBS and decreasing surface tension. The black lines show the effect of valve width (bottom abscissa) and diverging angle, denoted by the numbers to the right of the curves, on valve pressure at constant tween-20 concentration (0.001%) and height (170 μm). Increasing width decreases valve pressure and increasing diverging angle increases valve pressure. We experimentally determined that approximately 800 Pa of valve pressure drop was required to hold during ITP operation. We use a concentration of 0.001%, valve width of 75 μm, height of 170 μm, and β of 120° in our design for a valve pressure of approximately 900 Pa.

Separation capacity

The separation parameter, Q_s, and the separation capacity (also called the column hold-up), Q_L, determine whether two groups of ions can be separated using isotachophoresis.[3,4] The separation parameter is the amount of charge required to separate two groups of ions and the separation capacity is the amount of charge passed through a channel before the first group of ions reaches its final destination. If the separation capacity is greater than the separation parameter, the two ions should be completely separated by isotachophoresis. The separation parameter is given by,[3]

$$Q_S = F \cdot \frac{N_A(u_A - u_R) + N_B(u_B - u_R)}{u_A - u_B} \qquad (2)$$

where N_A and N_B are the amounts of ions to be separated, u_A, u_B, and u_R are the effective ionic mobilities of the two ions to be separated and the counter ion respectively, and F is Faraday's constant. For constant current operation, the separation capacity can be calculated using experiments by $Q_L = I(t_1 - t_0)$, where I is the current, and $(t_1 - t_0)$ is the time interval from the beginning of separation, t_0, to the end of separation, t_1 (*i.e.* when DNA enters the extraction chamber). We used the values given in Table S1 to calculate Q_s. The Q_L value was determined using experiments that typically required 4 minutes at 450 μA to complete, *i.e.* $Q_L = 240s \cdot 0.450mA = 108mC$. For designing systems, $Q_L = N_L F\left(1 - u_R / u_L\right)$, where N_L is the amount of leading electrolyte (mols) and u_L is the mobility of the leading electrolyte, can be used to determine the separation capacity. This calculation gives a value of 98.0 mC for our system.

Table S1. Values used to calculate the separation parameter according to equation 2, and the separation parameter and separation capacity results.

Component	N_i **(x10^7 mols)**	u_i **(x10^8 m^{2}V^{-1}s^{-1})**	Q_s **(mC)**	Q_L **(mC)**
A: DNA	0	-2.7	51.7	108.0 (experimental)
B: Fatty acids	7.0	-0.6		98.0 (calculated)
R: Tris ions	–	+1.0		

We assumed the fatty acids to be the fastest moving contaminant due to the high charge of triglycerides and the relatively low mobility of proteins, so the separation parameter is determined using the fatty acids in the milk. The number of moles of DNA is sufficiently small (approximately pico gram quantities of DNA with molecular weight >1 million) compared to the number of moles of fatty acids so that N_A can effectively be called zero for this calculation. The moles of fatty acids were calculated based off of 8 g of fat per serving of milk (240 mL), with 15 μL input and an assumed average molecular weight of 711 g/mol using the size of common triglyceride chains in cow's milk.[5] The fatty acid mobility was measured using a Malvern Zetasizer with 10% milk in TE buffer because 50% milk was too turbid to recover results. The mobility was corrected for ionic strength differences between 10% and 50% milk TE using SPRESSO open source simulation software.[6] The mobility of DNA in the TE buffer was determined using dilute mobility data from Stellwagen and Stellwagen and SPRESSO simulations to correct for ionic strength in our buffers.[7] The tris ion mobility was determined using SPRESSO.[6]

Hydraulic circuit calculations

We performed hydraulic circuit calculations to guide channel design.[8] Our goal was to have the valve burst, have preferential fluid flow from the extraction to the reaction chamber, and to isolate the reaction

chamber when the chip was heated to 65°C. The hydraulic resistances in the LE and ITP channels should be large relative to the valve burst pressure such that the pressure generated by heated air causes the valve to burst with only marginal flow through the LE and ITP channels. After bursting, liquid flow is driven by a combination of pressure driven flow and capillary flow. To quickly drive flow into the reaction chamber, the valve and reaction chamber should have lower resistance than the LE and ITP channels for preferential pressure driven flow towards the reaction chamber. Finally, the LE and ITP channels should have equal resistances to isolate the reaction chamber. Figure S3 shows a diagram of each channel considered as a resistor, R_i, that has a pressure applied to it, P_i, and corresponding volumetric flow Q_i. Channel 1 models the heated air chamber, channel 2 the LE channel, channel 3 the ITP channel, and channel 4 the reaction chamber. The resistance of each channel was calculated using $R_H \cong 8\eta L / r_H^2 A$, where η is the fluid viscosity, L is the channel length, $r_H = 2A / C$ is the hydraulic radius of the channel, A is the cross-sectional area of the channel, and C is the perimeter of the channel. Table S2 gives the pressures and dimensions for each channel of the optimized design. The flow rates for the given parameters were determined using a series of equations, $P_i = Q_i R_{Hi}$, where i denotes each channel.

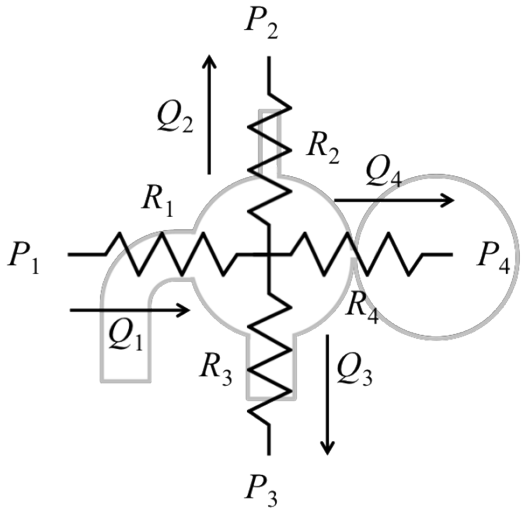

Figure S3. Schematic showing the resistor models for each channel with pressure, P, hydraulic resistance, R_H, and volumetric flow, Q. Channel 1 corresponds to the air chamber, channel 2 to the LE channel, channel 3 to the ITP channel, and channel 4 to the capillary valve and reaction chamber.

Table S2. Parameters used for each channel in the hydraulic circuit calculations.

	Channel 1	Channel 2	Channel 3	Valve (Channel 4)	Reaction chamber (channel 4)
P (Pa)	108730	101365	101365	N/A	101325
Height (μm)	170	170	170	170	170
Width (μm)	2000	125	600	75	1500
Length (mm)	0.1	4	50	0.1	2.5

The pressure for channel 1 is the mean of the air channel pressure immediately after heating to 65°C from room temperature and atmospheric pressure according to the ideal gas law. The pressure for channel 2 and 3 is atmospheric pressure plus the hydrostatic pressure from liquid in the inlets. Channel 4 considers the valve and reaction chamber as resistors in series because the air valve (atmospheric pressure) for channel 4 is located at the end of the reaction chamber. Based off the calculations using the parameters in Table S2, the hydraulic resistances for channel 2 and 3 are 2.6×10^{11} $Ns^{-1}m^{-5}$ and 2.5×10^{11} $Ns^{-1}m^{-5}$ respectively, and the volumetric flow through channel 4 should be 9.39 times greater than the LE channel, *i.e.* $Q_4/Q_2=9.39$, and 9.06 times greater than the ITP channel, *i.e.* $Q_4/Q_3=9.06$.

SEBS device fabrication

We fabricated the SU-8 silicon wafers using photolithography. An SU-8 2050 (Microchem, SU-8 2000 series) photoresist layer ~170 μm thick was spun (500 RPM for 5s, followed by 1250 RPM for 30s) onto a 4-in silicon wafer and prebaked for 20 min at 95°C. The resist was exposed to UV-light through a printed photomask (Fineline Imaging, Colorado Springs, CO) using an ABM contact aligner, baked again at 95 °C for 15 min, developed using SU-8 developer for 10 min (Microchem, Y020100, CAS: 108-65-6), and then hard-baked overnight at 150°C. An alpha step profilometer measured the height of the SU-8 microstructures, which correspond to the channel height. The master molds were silane coated by placing them in a desiccator under low vacuum for 30 min next to a Petri dish containing 50 μL of trichloro(1H,1H,2H,2H-perfluorooctyl)silane to create a nonstick surface for molding.

For SEBS fabrication, approximately 10 w/v% of SEBS was dissolved in toluene and mixed on a rotary mixer until the solution was transparent.[9] The solution was then sonicated for 2 h to further dissolve the polymer and placed under vacuum in a dessicator for two minutes to ensure there were no trapped air bubbles in the solution. We slowly poured the de-gassed solution through a funnel onto the patterned wafer inside a PTFE coated ring (Norpro 666, Everett, WA) and baked for 3h at 65°C and 10h at 90°C on a hotplate inside a fume hood. We heated the wafer to 40°C on a hotplate before de-molding to promote easier removal of the SEBS to protect the SU-8 structures.

LAMP primers

Table S3 lists the sequences for the six primers, F3, B3, forward inner primer (FIP), backward inner primer (BIP), loop forward (LF), and loop back (LB) used during LAMP amplification. The primers target the *eae* gene of *E. coli* O157:H7 and were developed by Wang et al.[17]

Table S3. Sequences of the six LAMP primers.

Primer Name	Sequence (5'–3')
F3	TGACTAAAATGTCCCCGG
B3	CGTTCCATAATGTTGTAACCAG
FIP	GAAGCTGGCTACCGAGACTC-CCAAAAGCAACATGACCGA
BIP	GCGATCTCTGAACGGCGATT-CCTGCAACTGTGACGAAG
LF	GCCGCATAATTTAATGCCTTGTCA
LB	ACGCGAAAGATACCGCTCT

LAMP reaction test results

Figure S3 shows various example images of tube-LAMP and NAIL LAMP reactions taken with mobile phone imaging and/or fluorescent microscopy imaging.

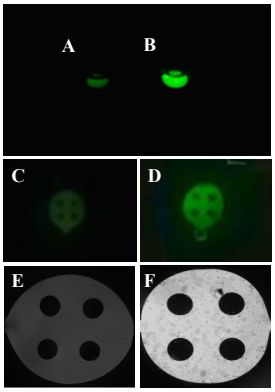

Figure S3. Example images of a (A) negative and (B) positive LAMP reaction with *E. coli* O157:H7 genomic DNA using mobile phone detection; (C) a negative NAIL and (D) positive NAIL reaction with mobile phone detection; and (E) a negative NAIL and (F) positive NAIL reaction with fluorescent microscopy detection.

Limit of detection plots with 95% confidence intervals

Figure S4 shows the NAIL limit of detection data from Figure 5 in the manuscript with 95% confidence intervals as the error bars instead of 1.645 times the standard deviation as shown in the manuscript. The 95% confidence intervals shows our confidence in creating an interval that contains the true mean and that the mean fluorescence for the tests conducted above the LoD are unambiguously larger than those conducted below the LoD.

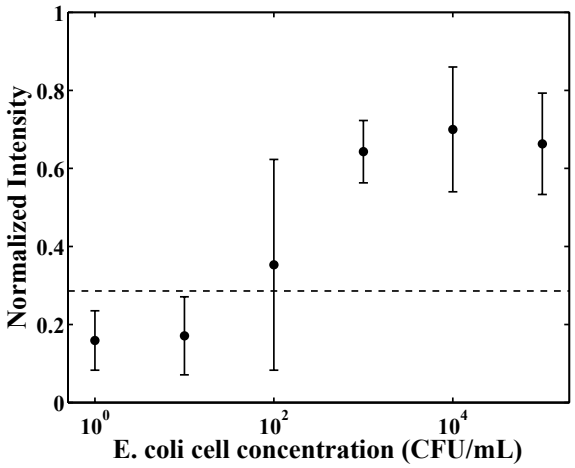

Figure S4. Normalized fluorescent intensity versus E. coli cell concentration (CFU/mL) for NAIL limit of detection tests with 95% confidence intervals as the error bars. The dotted line shows the threshold for determining positive (above the threshold) or negative (below the threshold) tests. Concentrations above 1000 CFU/mL show consistently positive positive results.

Summary of Limit of Detection results

Tables S4 and S5 show a summary of the milk dilution tube-LAMP tests (positive/total valid runs) and the NAIL and tube-LAMP limit of detection tests at various cell concentrations.

Table S4. Summary of results for the milk dilution tests with 100 pg of *E. coli* DNA. The number of correct results out of the total number of valid runs are given for each dilution.

Dilution	Results
10x	0/3
100x	1/5
200x	0/3
500x	2/3
1000x	5/5
10000x	3/3
Pure water	15/15

Table S5. Summary of LoD results for the NAIL and tube-LAMP tests with varying initial cell concentration levels in whole milk. The results are given as the number correct out of the total number of valid runs.

Initial cell concentration (CFU/mL)	NAIL	tube-LAMP
0	0/22	0/8
1	0/5	–
10^1	0/5	–
10^2	1/5	0/3
10^3	10/10	0/3
10^4	5/5	0/3
10^5	5/5	5/5
10^6	–	3/3

References

1 H. Cho, H.-Y. Kim, J. Y. Kang and T. S. Kim, *J. Colloid Interface Sci.*, 2007, **306**, 379–385.
2 M. R. R. Niño and J. R. Patino, *J. Am. Oil Chem. Soc.*, 1998, **75**, 1241–1248.
3 P. Bocek, M. Deml, B. Kaplanova and J. Janak, *J. Chromatogr.*, 1978, **160**, 1–9.
4 A. Rogacs, L. A. Marshall and J. G. Santiago, *J. Chromatogr. A*, 2014, **1335**, 105–120.
5 W. C. Breckenridge and A. Kuksis, *J. Lipid Res.*, 1967, **8**, 473–478.
6 M. Bercovici, S. K. Lele and J. G. Santiago, *J. Chromatogr. A*, 2009, **1216**, 1008–1018.
7 E. Stellwagen and N. C. Stellwagen, *Electrophoresis*, 2003, **23**, 1935–1941.
8 B. Kirby, *Micro- and nanoscale fluid mechanics transport in microfluidic devices*, Cambridge University Press, New York, 2010.
9 M. D. Borysiak, K. S. Bielawski, N. J. Sniadecki, C. F. Jenkel, B. D. Vogt and J. D. Posner, *Lab. Chip*, 2013, **13**, 2773–2784.
10 T. K. Khurana and J. G. Santiago, *Anal. Chem.*, 2008, **80**, 6300–6307.
11 A. Persat, R. D. Chambers and J. G. Santiago, *Lab. Chip*, 2009, **9**, 2437–2453.
12 A. Persat, M. E. Suss and J. G. Santiago, *Lab. Chip*, 2009, **9**, 2454.
13 D. Milanova, R. D. Chambers, S. S. Bahga and J. G. Santiago, *Electrophoresis*, 2011, **32**, 3286–3294.
14 G. Garcia-Schwarz, M. Bercovici, L. A. Marshall and J. G. Santiago, *J. Fluid Mech.*, 2011, **679**, 455–475.
15 D. Milanova, R. D. Chambers, S. S. Bahga and J. G. Santiago, *Electrophoresis*, 2012, **33**, 3259–3262.
16 M. D. Borysiak, E. Yuferova and J. D. Posner, *Anal. Chem.*, 2013, 11700–11704.
17 F. Wang, L. Jiang and B. Ge, *J. Clin. Microbiol.*, 2011, **50**, 91–97.